ARTICLE

CdS Magic-Sized Nanocrystals Exhibiting Bright Band Gap Photoemission *via* Thermodynamically Driven Formation

Minjie Li,[†,§,⊥] Jianying Ouyang,[†,⊥] Christopher I. Ratcliffe,[†] Laetitia Pietri,[†] Xiaohua Wu,[‡] Donald M. Leek,[†] Igor Moudrakovski,[†] Quan Lin,[§] Bai Yang,[§] and Kui Yu[†,*]

[†]Steacie Institute for Molecular Sciences, National Research Council of Canada, Ottawa, Ontario K1A 0R6, Canada, [‡]Institute for Microstructural Sciences, National Research Council of Canada, Ottawa, Ontario K1A 0R6, Canada, and [§]State Ley Lab for Supramolecular Structure and Materials, Jilin University, Changchun 130012, China. [⊥]These authors contributed equally to this work.

ABSTRACT CdS magic-sized nanocrystals (MSNs) exhibiting both band gap absorption and emission at 378 nm with a narrow bandwidth of ~9 nm and quantum yield (QY) of ~10% (total QY ~28%, in hexane) were synthesized *via* a one-pot noninjection approach. This CdS MSN ensemble is termed as Family 378. It has been acknowledged that magic-sized quantum dots (MSQDs) are single-sized, and only homogeneous broadening contributes to their bandwidth. The synthetic approach developed is ready and highly reproducible. The formation of the CdS MSQDs was carried out at elevated temperatures (such as 90—140 °C) for a few hours in a reaction flask containing bis(trimethylsilyl)sulfide ($(TMS)_2S$) and Cd(OAc)(OA) *in situ* made from cadmium acetate dihydrate ($Cd(OAc)_2 \cdot 2H_2O$) and oleic acid (OA) in 1-octadecene (ODE). Low OA/Cd and high Cd/S feed molar ratios favor this formation, whose mechanism is proposed to be thermodynamically driven. ^{13}C solid-state cross-polarization magic-angle spinning (CP/MAS) nuclear magnetic resonance (NMR) demonstrates that the capping ligands are firmly attached to the nanocrystal surface *via* carboxylate groups. With the cross-polarization from ^{1}H of the alkyl chains to surface ^{113}Cd, ^{113}Cd NMR is able to distinguish the surface Cd (471 ppm) bonding to both $-COO^-$ and S and the bulk Cd (792 ppm) bonding to S only. DOSY-NMR was used to determine the size of Family 378 (~1.9 nm). The present study provides strategies for the rational design of various MSNs.

KEYWORDS: CdS · single-sized nanocrystals · magic-sized nanocrystals (MSNs) · one-pot noninjection · band gap emission · homogeneous broadening

Colloidal semiconductor quantum dots (QDs) exhibiting band gap photoemission with narrow bandwidth have generated a great deal of interest in both fundamental and applied research over the past decade.[1−6] With significant recent progress, such QDs were synthesized either *via* hot-injection[7−10] or noninjection[11−18] approaches. The well-documented synthetic approaches usually led to regular QDs (RQDs), each ensemble of which consists of nanocrystals with a certain size distribution. Therefore, both homogeneous and inhomogeneous broadening contribute to the bandwidth of their absorption and emission.[19,20] Single-sized nanocrystals without the inhomogeneous spectral line broadening are also called magic-sized nanocrystals (MSNs), exhibiting single-dot optical properties. With proper surface passivation and high crystallinity, such MSNs could be expected to produce band gap emission.[21−26] The development of synthetic approaches to single-sized QDs with band gap photoemission is very challenging and has generated significant interest in our laboratories and others.[21−33] Although there were reports on CdS, CdSe, and CdTe nanoclusters or MSNs exhibiting narrow and persistent absorption peaks during synthesis, the resulting MSNs were not in pure form and/or did not exhibit narrow band gap emission but sometimes broad trap emission.[27−33] Recently, we were the first to report CdSe, CdTe, CdTeSe, and Cd_3P_2 MSNs having strong band gap emission synthesized in pure form by noninjection one-pot approaches;[21−25] the optical bandwidth in full width at half-maximum (fwhm) was only ~9, 10, 20, and 17 nm, respectively. We report here CdS MSNs exhibiting bright band gap emission from a one-pot noninjection approach that is thermodynamically driven. With low acid/Cd and high Cd/S feed molar ratios that were also applied to our syntheses to CdSe, CdTe, CdTeSe, and Cd_3P_2 MSNs,[21−25] a family of CdS MSNs was reproducibly synthesized in pure form (without the coexistence of regular QDs and other families of MSNs). This ensemble is labeled as Family 378, due to its sharp band gap absorption and narrow band gap emission both peaking at 378 nm. Oleic acid (OA) was used as the acid and subsequently capping ligand.

RESULTS AND DISCUSSION

Figure 1 shows the as-synthesized CdS MSN Family 378. The fwhm is as narrow as 9 nm. The nearly zero nonresonant Stokes

*Address correspondence to kui.yu@nrc.ca.

Received for review August 5, 2009 and accepted November 5, 2009.

Published online November 13, 2009. 10.1021/nn9009455

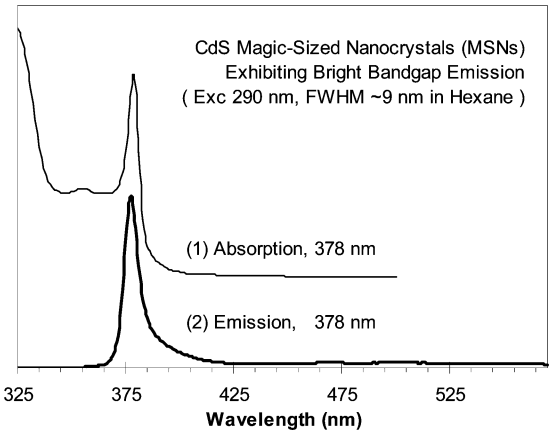

Figure 1. Absorption (1) and emission (2) spectra of CdS MSN Family 378 dispersed in hexane; the excitation wavelength was 290 nm. The MSNs were synthesized from a batch with the feed molar ratio of 2OA/4Cd/1S and the S concentration of ~33 mmol/L; the growth was carried out at 110 °C for 80 min.

shift (NRSS) and the negligible trap emission indicate the well-defined structure of this CdS MSN Family 378. The nanocrystals exhibited good storage stability, as shown in Supporting Information Figure S1.

Note that the fwhm is ~78 meV for Family 378 peaking at 378 nm with fwhm of ~9 nm. For the CdS RQDs from our similar noninjection-based approach, the fwhm is ~131 meV when one ensemble peaks at 401 nm (absorption) with photoemission fwhm of ~17 nm.[18] It is known that a dye molecule has a large line width due to strong vibrational coupling. For QDs, the homogeneous line width of one dot is related to exciton−phonon coupling; ~50 meV fwhm was reported for a CdSe/ZnS QD at room temperature.[19,20] A large QD has relatively small line width. However, the line width of one nanocrystal ensemble depends on many factors such as the composition, size, size distribution, dispersion medium, and temperature; it is commonly acknowledged that narrow size distribution leads to small fwhm. The Stokes shift of one nanocrystal ensemble is still an open question, regarding what factors contribute to the Stokes shift. For one nanocrystal, the Stokes shift seems to correlate with the line width; the narrower the line width, the smaller the Stokes shift.

Figure 2 shows the typical formation of our CdS MSNs *via* one-pot noninjection synthesis. Experimentally, cadmium acetate dihydrate ($Cd(OAc)_2 \cdot 2H_2O$) was reacted with oleic acid (OA) in 1-octadecene (ODE) at 120−130 °C under vacuum; afterward, bis(trimethylsilyl)sulfide ($(TMS)_2S$) was added into the reaction mixture, which was cooled to 60 °C under purified nitrogen. Then, the reaction system was heated at ~2 °C/min, and sampling was carried out at elevated temperatures such as 90−140 °C. Family 378 in pure form was obtained after 180 min growth at 100 °C (samples 11−13). Note that the significant coexistence of various families before sample 11 leads to broad absorption. The formation of the CdS nanocrystals could be achieved at low temperature such as 90 °C, due to the high reactivity of $(TMS)_2S$. Under our experimental conditions and time scale, each ensemble taken from 0 min/90 °C (curve 1) to 120 min/100 °C (curve 10) exhibited multiple absorption peaks. However, the relative absorbance ratios were not fixed; these peaks did not result from the electronic transitions (between the different states) of one CdS species. Therefore, several CdS species coexisted for each of these early stage ensembles, with their persistent absorptions peaking at ~322, 344−351, ~362, and 378 nm. The growth of the CdS nanocrystals was sequentially accompanied by the decreased absorption at 344−351 nm and the increased absorption at 362 nm, and the absorption at 362 nm started to reduce and the absorption at 378 nm continued to increase. Such change of the absorption does not necessarily suggest the growth of the small species into the next large one[31] but more likely the dissociation of the small species into the reactants to facilitate the formation of the next family.[21,22]

Our systematic studies have shown that the growth of the CdS MSNs was favored with low OA/Cd and high Cd/S feed molar ratios, which is in agreement with the growth of the other MSNs.[21−25] As demonstrated in Figures 1 and 2, high-quality CdS MSN Family 378 in pure form with bright band gap emission and little trap emission was indeed achieved with the feed molar ratios of 2OA/4Cd/1S. The thorough investigation on the effects of the acid/Cd and Cd/S feed molar ratios and the reactant concentration affecting the formation of CdS MSQD Family 378 is shown in Supporting Information Figures S2, S3, and S4, respectively. The formation

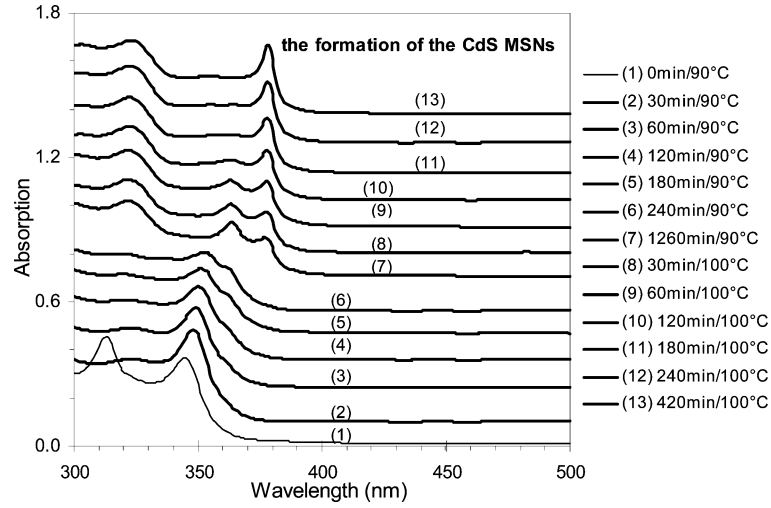

Figure 2. Kinetics of the formation of CdS MSN Family 378 monitored by the temporal evolution of the absorption (offset) of the growing CdS nanocrystals from a synthetic batch, similar to that shown in Figure 1, with the feed molar ratio of 2OA/4Cd/1S and [S] 34 mmol/L. The stepwise heating is indicated with the growth periods/temperature. The spectra were collected with the as-synthesized nanocrystals of 10 μL in 1 mL of hexane.

of the MSNs with our noninjection approaches is driven thermodynamically. The existing models of nucleation/growth, which deal with the formation of regular QDs with size distribution *via* hot-injection approaches do not apply to our MSNs.[34] For our MSNs *via* our noninjection syntheses, the underlying mechanism may be related to the slow release of Cd^{2+} in ODE from the unique Cd precursor Cd(OAc)(OA) and the enhanced thermal stability of the MSNs under high Cd^{2+} concentrations. Such an explanation could be illustrated more clearly with our recently developed model expressed as

$$Cd(OAc)_2{\cdot}2H_2O + OA \xrightarrow{1} Cd(OAc)(OA) \xrightarrow{2} Cd^{2+}$$

$$(TMS)_2S \xrightarrow{3} S^{2-}$$

$$Cd^{2+} + S^{2-} \overset{4}{\rightleftarrows} (CdS)_n(MSQD)$$

The Cd precursor Cd(OAc)(OA), generated by step 1 with low acid/Cd feed molar ratios, was so unique that it slowly released reactant Cd^{2+} (step 2) due to its limited solubility in ODE. Reaction step 2, thus, became the rate-limiting step. Note that Cd^{2+} (step 2) and S^{2-} (step 3) are only simplified symbols for the reactant species (shown in step 4) without the emphasis of their associated counterions. $(CdS)_n$ magic-sized quantum dots (MSQDs) have a local maximum in binding energy, and their formation was thermodynamically driven.[30,35] Note that MSQDs can only change in number but not in size;[21−25] they were also termed as magic-sized nuclei.[36,37]

Accordingly, it is easy to understand that low acid/Cd feed molar ratios ensure the formation of the Cd(OAc)(OA) precursor and thus a slow and controlled release of Cd^{2+}. High Cd/S feed molar ratios ensure relatively high $[Cd^{2+}]$ and thus drive step 4 to the direction of the formation of $(CdS)_n$ and prevent the dissociation of $(CdS)_n$ formed. The Cd^{2+} release and its reactivity, which determine *n*, are controlled by parameters including the nature of the ligand used (type, length, and amount) and reaction temperature. We have already demonstrated that short-chain acids favor the formation of small-sized CdSe MSQDs, while long-chain ligands favor large-sized ones.[21] As shown in Figure 3, another relatively small-sized family of CdS MSQDs was formed by substituting OA with octanoic acid; this family is labeled as Family 324 according to its persistent absorption peaking at 324 nm. According to the empirical relation between absorption and size,[38] Family 324 is very small with its dimension of ~1.6 nm. The present study focuses only on OA-capped CdS MSQD Family 378.

The characterization of CdS MSN Family 378 by nuclear magnetic resonance spectroscopy (NMR), X-ray

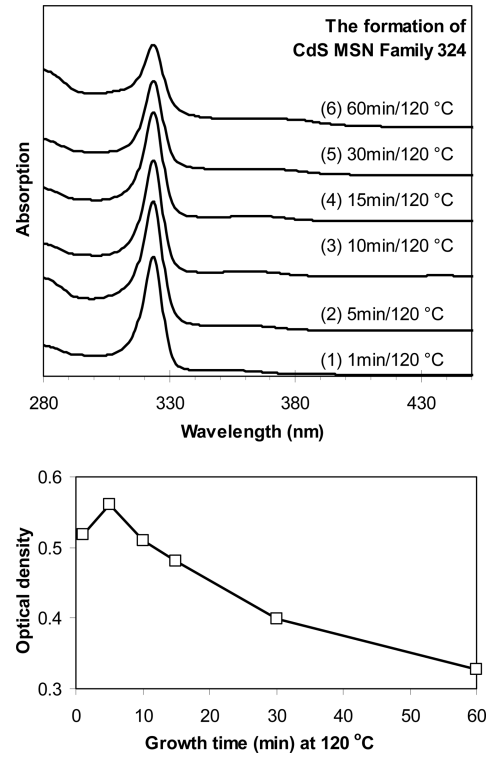

Figure 3. (Top) Formation kinetics of CdS MSN Family 324 monitored by the temporal evolution of the absorption (offset) of the growing CdS nanocrystals from a synthetic batch with the feed molar ratio of 2OA/4Cd/1S and [S] 33 mmol/L. The growth periods/temperature are indicated. The sample concentration was constant with 10 μL of crude reaction mixture dispersed in 3.0 mL of hexane. (Bottom) Optical density at 324 nm of the six corresponding samples shown in the top of the figure. It is obvious that the optical density increased first and then decreased; such change indicates an increase of Family 324 in number and then a decrease in number.[38]

diffraction spectroscopy (XRD), and transmission electron microscopy (TEM) was carried out with purified samples. The purification procedure did not lead to the change of the nanocrystals significantly, as shown in Supporting Information Figure S5. Solid-state NMR is a powerful technique for providing information on both the surface and the core of QDs. For the nanocrystal surface, it is about the binding nature between surface atoms and ligands and the surface-to-core structural change. For the nanocrystal core, it is about the composition and compositional change.[21−25] Figures 4 and 5 show the solid-state ^{113}Cd and ^{13}C NMR spectra, respectively. Except for increased shifts, the ^{113}Cd spectra appear very similar to those observed previously for the CdSe, CdTeSe, CdTe, and Cd_3P_2 MSNs,[21−25] and assignments can be made using the same reasoning as for those. There are two main resonances: one with an isotropic shift of ~471 ppm assigned to surface Cd, the other with an isotropic chemical shift of ~792 ppm, assigned to core Cd. The former has a large chemical shift anisotropy (CSA) which gives rise to multiple prominent spinning side bands (ssbs). The latter does not have any significant ssbs due to the roughly tetra-

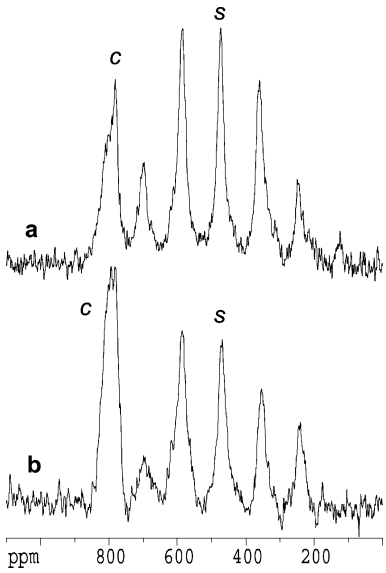

Figure 4. ^{113}Cd MAS NMR spectra of CdS MSN Family 378 acquired with CP/MAS (a) and high-power decoupling (HPDEC) (b). The core Cd is labeled with *C* and the surface Cd is labeled with *S*.

hedral coordination to four S atoms, which ensures that the CSA is small. Furthermore, the surface-to-core intensity ratio of the two resonances is larger in the cross-polarization (CP) spectrum (Figure 4a) than that in the high-power decoupling (HPDEC) spectrum (Figure 4b). Since the surface Cd atoms are partly coordinated by carboxylate anions and are closest to the H atoms of the carboxylate chain, they cross-polarize more readily than the core Cd. It is noteworthy that the OA-capped CdS RQDs from a similar noninjection approach show the core Cd at ~808 ppm (shown in Supporting Information Figure S6). The difference in the chemical shift of the core Cd of the MSNs and RQDs may be related to the expansion of the crystal unit of the MSNs (as shown in Figure 6.

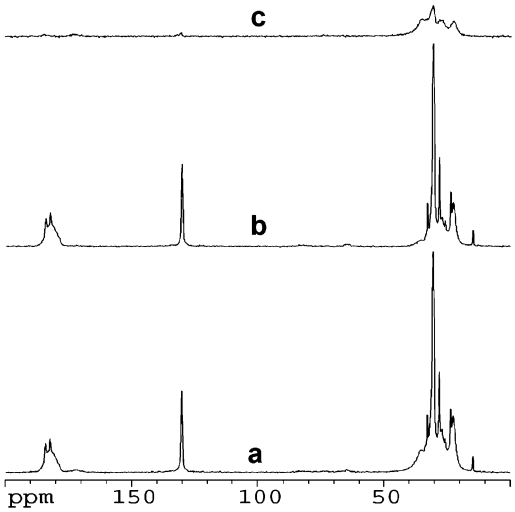

Figure 5. ^{13}C CP MAS NMR spectra of CdS MSN Family 378: normal (a), dipolar dephased (b), and difference (c).

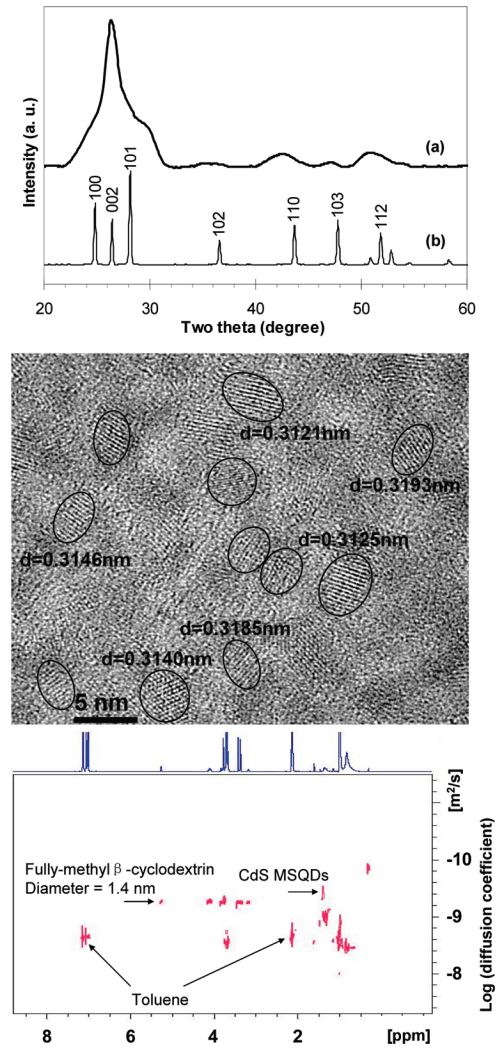

Figure 6. (Top) Powder XRD patterns of CdS MSN Family 378 (a) and the bulk hexagonal CdS (b). The diffraction peaks are indexed. (Middle) Typical TEM image of CdS MSN Family 378. The lattice is clearly seen as highlighted, and some *d* spacing values are indicated. The scale bar is 5 nm. (Bottom) ^{1}H DOSY-NMR spectrum of CdS MSQD Family 378 in toluene-d_8.

The normal ^{13}C CP MAS spectrum is shown in Figure 5a. The appearance of some of the protonated carbon resonances in the dipolar dephased spectrum (Figure 5b) indicates a significant amount of motion in the oleate anion chain, including the olefinic carbons (130.2 ppm) halfway along the chain. Nevertheless, in the difference spectrum (Figure 5c), it is clear that some CH_2 groups are not in motion. Presumably, as for other carboxylate anion surface ligands,[15,21−25] the $-COO^-$ group is coordinated to the surface Cd and those CH_2 closest to the $-COO^-$ group are essentially rigid.

Figure 6 (top) shows the XRD patterns of Family 378 and bulk hexagonal wurtzite CdS. The CdS MSNs have a hexagonal crystal structure, as indicated by the presence of the characteristic diffraction peaks such as (102) and (103) planes. The hexagonal crystal structure suggests that the MSNs are thermodynamically stable products; usually, noninjection approaches lead to

nanocrystals with a cubic crystal structure,[11−18] and the cubic-to-hexagonal phase transition was documented for CdS and CdSe nanocrystals with thermal annealing at 300−400 °C.[39] Significantly, the diffraction peaks of the MSNs shift to the low-angle direction relative to the those of the bulk CdS; for example, the resolved diffraction peaks of (102), (110), (103), and (112) planes decrease in 2θ by ∼0.80−0.99°. Such decreases in 2θ suggest the increase in the lattice parameters of the MSNs: a from 4.145 to 4.237 Å and c from 6.719 to 6.907 Å. Similar increases in the lattice parameters were reported also for the CdSe nanoclusters of ∼2 nm in diameter;[40] the expansion in the crystal unit of those magic-sized nanoclusters was argued to be the geometry optimization for the stable structure required.[40,41] Interestingly, the (002) diffraction peak of the CdS MSNs is noticeably sharper than the other peaks, indicating significant elongation along some preferred directions such as [002].[21−24] The size is calculated to be ∼3.65 nm using the Sherrer equation,[42] based on the (110) diffraction peak.

Figure 6 (middle) shows a typical high-resolution TEM image of the CdS MSNs with high crystallinity. The averaged *d* spacing value of 3.1−3.2 Å was obtained, which agrees with the characteristic *d* spacing value of 3.16 Å for (101) plane of bulk hexagonal CdS.[43] The TEM image suggests the size of 3−4 nm, while the 378 nm absorption suggests ∼2.7 nm.[38] It has been acknowledged that the size determination of small QDs (smaller than 2 nm) is challenging. At present, each available technique has its own limitations.[44] In addition, considerable aggregation and/or coalescence of the MSQDs took place during the XRD and TEM sample preparation with solvent evaporation.[21−25] TEM and XRD are not solution-based techniques.

Therefore, a solution-based technique without solvent evaporation induced aggregation, diffusion-ordered spectroscopy (DOSY) NMR, was explored to characterize the size of CdS MSQD Family 378. Figure 6 (bottom) shows the DOSY spectrum of CdS MSQD Family 378 in toluene-d_8. The average diffusion coefficient of the MSQDs was measured to be $\sim 10^{-9.410}$ m^2/s, with $10^{-9.275}$ m^2/s from an internal standard heptakis (2,3,6-tri-*o*-methyl)-β-cyclodextrin (average diameter 1.4 nm); thus, the size is estimated to be ∼1.9 nm.[21−24] It is necessary to point out that such effort on determining the size of Family 378 was significant. A well-characterized nanocluster of $Cd_{32}S_{50}$ was reported to have a CdS core with 82 atoms and the overall size of 1.5 nm, while exhibiting band gap absorption peaking at 358 nm.[27] Family 378 should contain more Cd and S atoms with its size larger than 1.5 nm.

CONCLUSION

In summary, CdS MSN Family 378 was synthesized in pure form *via* a thermodynamically driven formation with a noninjection one-pot approach. Family 378 exhibits band gap absorption and emission at 378 nm with a narrow bandwidth of 9 nm in fwhm. The growth of the CdS MSQDs was favored with low OA/Cd and high Cd/S feed molar ratios. The NMR study indicated that the capping carboxylate groups are firmly attached to the nanocrystals, and the surface and core Cd atoms could be distinguished accordingly. A hexagonal wurtzite crystal structure was determined by XRD and TEM, and the DOSY NMR suggested a size of ∼1.9 nm.

EXPERIMENTAL SECTION

All chemicals used are commercially available and were used as received: cadmium acetate dihydrate (Alfa Aeser, $Cd(OAc)_2 \cdot 2H_2O$, 99.999%), bis(trimethylsilyl)sulfide (Fluka, $(TMS)_2S$), oleic acid (Aldrich, OA, tech. 90%), octanoic acid (Aldrich, ≥ 98%), and 1-octadecene (Aldrich, ODE, tech. 90%), hexane (EMD, ≥98.5%), toluene (ACP, ≥99.5%), 2-methylbutane (Sigma-Aldrich, ≥99%), 1-butanol (Aldrich, 99.5%).

A typical synthesis with the feed molar ratio of 2OA/4Cd/1S was carried out as follows: 0.8 mmol $Cd(OAc)_2 \cdot 2H_2O$ and 0.4 mmol OA were heated in 3.9 mL of ODE in a three-neck round flask equipped with an air condenser connected to a Schlenk line at ∼120 °C under vacuum (∼50 mTorr) for 3 h. Then, 0.2 mmol $(TMS)_2S$ diluted in 2.0 mL of ODE was added to the above solution at 60 °C under a flow of nitrogen. CdS nanocrystals were obtained at an elevated temperature with nonstop heating or stepwise heating, with a rate of ∼2 °C/min. To monitor the formation of the nanocrystals, a small amount of aliquots (∼0.2 mL) was quickly taken from the reaction mixture.

For the optical measurements, the as-synthesized nanocrystal samples were dispersed in hexane or toluene at room temperature. Ultraviolet−visible (UV−vis) absorption spectra were collected using a 1 nm data collection interval (Perkin-Elmer Lambda 45 spectrometer). Photoemission spectra were collected with the excitation wavelength 300 and/or 350 nm, an increment of data collection of 1 nm, and the slits of 3 nm (Fluoromax-3 spectrometer, Jobin Yvon Horiba, Instruments SA, with a 450 W Xe lamp as the excitation source). Gaussian-fitted and baseline-subtracted integration were performed using built-in Fluoromax3 software functions to yield emission peak position, width (fwhm, in nm), and area (intensity). The PL quantum yield was estimated by comparing the integrated emission of a given nanocrystal sample in dilute hexane or toluene solution with an optical density ∼0.1 (at the excitation wavelength) with that of quinine sulfate in 0.05 M H_2SO_4 (lit. QY = 0.546), together with the correction of the difference of the refractive index of the solvents, namely, hexane or toluene and water.

The CdS MSNs were purified as follows: ∼3 mL of 2-methylbutane was added to ∼3 mL of the raw reaction product of CdS MSNs. After centrifuging, the supernatant contained the nanocrystals, while the bottom part, namely, the precipitate (with the unreacted Cd source and/or Cd precursor), was removed. 1-Butanol was added dropwise until the supernatant became turbid, and then 20% more 1-butanol was added; after centrifuging, the precipitate was collected. The purification was repeated once or twice. The purified sample was used for XRD, TEM, and NMR characterization.

Transmission electron microscopy (TEM) sample was prepared by depositing diluted purified nanocrystal dispersion in toluene onto a 300-mesh carbon-coated TEM copper grid and allowed to air-dry. TEM images were collected on a JEOL JEM-2100F electron microscope operating at 200 kV and equipped with a Gatan UltraScan 1000 CCD camera. The *d* spacing was measured with built-in software.

The powder X-ray diffraction (XRD) sample was prepared by depositing the purified nanocrystals on a low-background quartz

plate. The XRD patterns were recorded at room temperature on a Bruker AXS D8 X-ray diffractometer using Cu Kα radiation in a θ−θ mode. The generator was operated at 40 kV and 40 mA, with data collected between 5 and 80° in 2θ mode, a step size of 0.1°, and a counting time of 5 s per step. The size of Family 378 was calculated based on the (110) peak in the XRD spectrum (Figure 6 (top)) using the Scherrer equation: $d = \kappa\lambda/\beta \cos\theta$, where κ is a constant (taken as 0.9 here), λ is the X-ray wavelength, which is 0.154 nm here (Cu Kα); while β and θ are the fwhm (in radians) and the Bragg angle, which are 0.0407 and 21.32°, respectively. The calculated size is ~3.65 nm.

For diffusion-ordered spectroscopy (DOSY) NMR, the study was performed with a Bruker DRX-400 spectrometer equipped with an inverse detected Z-gradient probe. The crude product of Family 378 was purified with two rounds of toluene/isopropanol; afterward, the purified CdS MSNs were dried in air and dispersed in toluene-d_8. Diffusion coefficients were measured using standard Bruker pulse sequences. In order to meet the accuracy requirements for parameters such as the sample viscosity and the temperature, an internal standard was used, which was heptakis(2,3,6-tri-*o*-methyl)-β-cyclodextrin with an average diameter of 1.4 nm. According to the Stokes−Einstein equation, the diffusion coefficient of a particle is inversely proportional to its diameter; thus, the nanocrystal size can be obtained readily from the ratio of its diffusion coefficient to that of the internal standard. In Figure 6 (bottom), heptakis(2,3,6-tri-*o*-methyl)-β-cyclodextrin shows a diffusion coefficient of $10^{-9.275}$ m^2 s^{-1}, and toluene exhibits resonances at 7.10−6.95 and 2.09 ppm with a diffusion coefficient of $10^{-8.650}$ m^2 s^{-1}. Family 378 shows an average diffusion coefficient of $10^{-9.410}$ m^2 s^{-1} (in the range of $10^{-9.300}$ and $10^{-9.550}$); thus, the average size was determined to be $1.4 \times (10^{-9.275}/10^{-9.410}) = 1.91$ nm (in the range of 1.4−2.7 nm).

For the solid-state NMR studies, the spectra were obtained on a Bruker DSX-400 spectrometer with a BL4 probe and 4 mm ZrO_2 spinners. ^{113}Cd NMR magic-angle spinning (MAS) spectra were obtained at 88.84 MHz, both with and without ^{1}H cross-polarization (CP). CP and one-pulse high-power proton decoupled (HPDEC) spectra were recorded under MAS at 10−12.5 kHz. The delay time for the ^{113}Cd HPDEC MAS spectra was 120 s, and about 1200 scans were accumulated to obtain acceptable signal-to-noise ratio (~40 h). ^{113}Cd CP MAS spectra were obtained with a CP time of 5 ms, a recycle time of 2 s, and a total of 40 000 scans were acquired (~22 h). The isotropic line at ~471 ppm was identified by increasing the spinning rate, which causes only the spinning side bands to shift. Standard ^{13}C CP MAS spectra at 100.67 MHz were recorded with a CP time of 2 ms, 2 s recycle time, and about 8000 scans. Dipolar dephased ^{13}C CP MAS was obtained with an interruption of ^{1}H decoupling of 40 μs before data acquisition (referenced to TMS *via* external hexamethylbenzene). All spectra were obtained at room temperature, and chemical shifts were referenced to $Cd(NO_3)_2 \cdot 4H_2O$ (^{113}Cd, powdered, under MAS) and tetramethylsilane (^{13}C). The sample for solid-state NMR was synthesized with a 3-time scale of the typical synthesis and the growth temperature of 140 °C with a non-stop heating program.

Acknowledgment. M.L. thanks the China Scholarship Council for financial support and the Chinese Ministry of Education in Ottawa and NRC International Relations Office for assistance. K.Y. thanks Programme of Introducing Talents of Discipline to Universities (111 Project). We thank Dr. Badruz Md. Zaman and Dr. Ruibing Wang for useful discussion.

Supporting Information Available: Storage stability of CdS MSN Family 378, the formation of Family 378 affected by synthetic parameters including various OA/Cd and Cd/S feed molar ratios and reactant concentrations, the optical properties before and after purification, and ^{113}Cd MAS solid-state NMR spectra of CdS MSN and RQDs. This material is available free of charge *via* the Internet at http://pubs.acs.org.

REFERENCES AND NOTES

1. Bruchez, M., Jr.; Moronne, M.; Gin, P.; Weiss, S.; Alivisatos, A. P. Semiconductor Nanocrystals as Fluorescent Biological Labels. *Science* **1998**, *281*, 2013–2016.
2. Chan, W. C. W.; Nie, S. Quantum Dot Bioconjugates for Ultrasensitive Nonisotopic Detection. *Science* **1998**, *281*, 2016–2018.
3. Medintz, I. L.; Uyeda, H. T.; Goldman, E. R.; Mattoussi, H. Quantum Dot Bioconjugates for Imaging, Labelling and Sensing. *Nat. Mater.* **2005**, *4*, 435–446.
4. Mueller, A. H.; Petruska, M. A.; Achermann, M.; Werder, D. J.; Akhadov, E. A.; Koleske, D. D.; Hoffbauer, M. A.; Klimov, V. I. Multicolor Light-Emitting Diodes Based on Semiconductor Nanocrystals Encapsulated in GaN Charge Injection Layers. *Nano Lett.* **2005**, *5*, 1039–1044.
5. Saunders, B. R.; Turner, M. L. Nanoparticle−Polymer Photovoltaic Cells. *Adv. Colloid Interface Sci.* **2008**, *138*, 1–23.
6. Zaman, M. B.; Baral, T.; Zhang, J.; Whitfield, D.; Yu, K. Single-Domain Antibody Functionalized CdSe/ZnS Quantum Dots for Cellular Imaging of Cancer Cells. *J. Phys. Chem. C* **2009**, *133*, 496–499.
7. Murray, C. B.; Norris, D. J.; Bawendi, M. G. Synthesis and Characterization of Nearly Monodisperse CdE (E = S, Se, Te) Semiconductor Nanocrystallites. *J. Am. Chem. Soc.* **1993**, *115*, 8706–8715.
8. Peng, Z. A.; Peng, X. Formation of High-Quality CdTe, CdSe, and CdS Nanocrystals Using CdO as Precursor. *J. Am. Chem. Soc.* **2001**, *123*, 183–184.
9. Yu, W. W.; Peng, X. Formation of High-Quality CdS and Other II−VI Semiconductor Nanocrystals in Noncoordinating Solvents: Tunable Reactivity of Monomers. *Angew. Chem., Int. Ed.* **2002**, *41*, 2368–2371.
10. Yu, K.; Zaman, M. B.; Singh, S.; Wang, D.; Ripmeester, J. A. The Effect of Dispersion Media on Photoluminescence of Colloidal CdSe Nanocrystals Synthesized from TOP. *Chem. Mater.* **2005**, *17*, 2552–2561.
11. Cao, Y. C.; Wang, J. One-Pot Synthesis of High-Quality Zinc-Blende CdS Nanocrystals. *J. Am. Chem. Soc.* **2004**, *126*, 14336–14337.
12. Yang, Y. A.; Wu, H.; Williams, K. R.; Cao, Y. C. Synthesis of CdSe and CdTe Nanocrystals without Precursor Injection. *Angew. Chem., Int. Ed.* **2005**, *44*, 6712–6715.
13. Chen, O.; Chen, X.; Yang, Y.; Lynch, J.; Wu, H.; Zhuang, J.; Cao, Y. C. Synthesis of Metal-Selenide Nanocrystals Using Selenium Dioxide as the Selenium Precursor. *Angew. Chem.* **2008**, *120*, 8766–8769.
14. Li, L.; Reiss, P. One-pot Synthesis of Highly Luminescent InP/ZnS Nanocrystals without Precursor Injection. *J. Am. Chem. Soc.* **2008**, *130*, 11588–11589.
15. Ouyang, J.; Ratcliffe, C. I.; Kingston, D.; Wilkinson, B.; Kuijper, J.; Wu, X.; Ripmeester, J. A.; Yu, K. Gradiently Alloyed $Zn_xCd_{1-x}S$ Colloidal Photoluminescent Quantum Dots Synthesized *via* a Noninjection One-Pot Approach. *J. Phys. Chem. C* **2008**, *112*, 4908–4919.
16. Liu, T.-Y.; Li, M.; Ouyang, J.; Zaman, Md. B.; Wang, R.; Wu, X.; Yeh, C.-S.; Lin, Q.; Yang, B.; Yu, K. Non-injection and Low-Temperature Approach to Colloidal Photoluminescent PbS Nanocrystals with Narrow Bandwidth. *J. Phys. Chem. C* **2009**, *113*, 2301–2308.
17. Ouyang, J.; Vincent, M.; Descours, P.; Boivineau, T.; Kingston, D.; Zaman, Md. B.; Wu, X.; Yu, K. Noninjection, One-Pot Synthesis of Photoluminescent Colloidal Homogeneously Alloyed CdSeS Quantum Dots. *J. Phys. Chem. C* **2009**, *113*, 5193–5200.
18. Ouyang, J.; Kuijper, J.; Brot, S.; Kingston, D.; Wu, X.; Leek, D. M.; Hu, M. Z.; Yu, K. Photoluminescent Colloidal CdS Nanocrystals with High Quality *via* Noninjection One-Pot Synthesis in 1-Octadecene. *J. Phys. Chem. C* **2009**, *113*, 7579–7593.
19. Empedocles, S. A.; Neuhauser, R.; Shimizu, K.; Bawendi, M. G. Photoluminescence from Single Semiconductor Nanostructures. *Adv. Mater.* **1999**, *11*, 1243–1256.
20. Schlegel, G.; Bohnenberger, J.; Potapova, I.; Mews, A. Fluorescence Decay Time of Single Semiconductor Nanocrystals. *Phys. Rev. Lett.* **2002**, *88*, 137401.
21. Ouyang, J.; Zaman, B.; Yan, F.; Johnston, D.; Li, G.; Wu, X.; Leek, M. D.; Ratcliffe, C. I.; Ripmeester, J. A.; Yu, K. Multiple Families of Magic-Sized CdSe Nanocrystals with Strong

Bandgap Photoluminescence via Noninjection One-Pot Syntheses. *J. Phys. Chem. C* **2008**, *112*, 13805–13811.
22. Yu, K.; Ouyang, J.; Zaman, B.; Johnston, D.; Yan, F.; Li, G.; Ratcliffe, C. I.; Leek, M. D.; Wu, X.; Stupak, J.; *et al.* Single-Sized CdSe Nanocrystals with Bandgap Photoemission *via* a Noninjection One-Pot Approach. *J. Phys. Chem. C* **2009**, *113*, 3390–3401.
23. Wang, R.; Ouyang, J.; Nikolaus, S.; Brestaz, L.; Zaman, Md. B.; Wu, X.; Leek, M. D.; Ratcliffe, C. I.; Yu, K. Single-Sized Colloidal CdTe Nanocrystals with Strong Bandgap Photoluminescence. *Chem. Commun.* **2009**, 962–964.
24. Wang, R.; Calvignanello, O.; Ratcliffe, C. I.; Wu, X.; Leek, D. M.; Zaman, Md. B.; Kingston, D.; Ripmeester, J. A.; Yu, K. Homogeneously-Alloyed CdTeSe Single-Sized Nanocrystals with Bandgap Photoluminescence. *J. Phys. Chem. C* **2009**, *113*, 3402–3408.
25. Wang, R.; Ratcliffe, C. I.; Wu, X.; Voznyy, O.; Tao, Y.; Yu, K. Magic-Sized Cd_3P_2 II−V Nanoparticles Exhibiting Bandgap Photoemission. *J. Phys. Chem. C* **2009**, *113*, 17979–17982.
26. Ithurria, S.; Dubertret, B. Quasi 2D Colloidal CdSe Platelets with Thicknesses Controlled at the Atomic Level. *J. Am. Chem. Soc.* **2008**, *130*, 16504–16505.
27. Herron, N.; Calabrese, J. C.; Farneth, W. E.; Wang, Y. Crystal Structure and Optical Properties of $Cd_{32}S_{14}(SC_6H_5)_{36} \cdot DMF_4$, a Cluster with a 15 Angstrom CdS Core. *Science* **1993**, *259*, 1426–1428.
28. Vossmeyer, T.; Reck, G.; Katsikas, L.; Haupt, E. T. K.; Schulz, B.; Weller, H. A "Double-Diamond Superlattice" Build up of $Cd_{17}S_4(SCH_2CH_2OH)_{26}$ Clusters. *Science* **1995**, *267*, 1476–1479.
29. Ptatschek, V.; Schmidt, T.; Lerch, M.; Müller, G.; Spanhel, L.; Emmerling, A.; Fricke, J.; Foitzik, A. H.; Langer, E. Quantized Aggregation Phenomena in II−VI-Semiconductor Colloids. *Ber. Bunsen-Ges. Phys. Chem.* **1998**, *102*, 85–95.
30. Kasuya, A.; Sivamohan, R.; Barnakov, Y. A.; Dmitruk, I. M.; Nirasawa, T.; Romanyuk, V. R.; Kumar, V.; Mamykin, S. V.; Tohji, K.; Jeyadevan, B.; *et al.* Ultra-Stable Nanoparticles of CdSe Revealed from Mass Spectrometry. *Nat. Mater.* **2004**, *3*, 99–102.
31. Kudera, S.; Zanella, M.; Giannini, C.; izzo, A.; Li, Y.; Gigli, G.; Cingolani, R.; Ciccarella, G.; Spahl, W.; Parak, W. J.; *et al.* Sequential Growth of Magic-Size CdSe Nanocrystals. *Adv. Mater.* **2007**, *19*, 548–552.
32. Kuçur, E.; Ziegler, J.; Nann, T. Synthesis and Spectroscopic Characterization of Fluorescent Blue-Emitting Ultrastable CdSe Clusters. *Small* **2008**, *4*, 883–887.
33. Evans, C. M.; Guo, L.; Peterson, J. J.; Maccagnano-Zacher, S.; Krauss, T. D. Ultrabright PbSe Magic-Sized Clusters. *Nano Lett.* **2008**, *8*, 2896–2899.
34. Rempel, J. Y.; Bawendi, M. G.; Jensen, K. F. Insights into the Kinetics of Semiconductor Nanocrystal Nucleation and Growth. *J. Am. Chem. Soc.* **2009**, *131*, 4479–4489.
35. Troparevsky, M. C.; Kronik, L.; Chelikowsky, J. R. *Ab Initio* Absorption Spectra of CdSe Clusters. *Phys. Rev. B* **2001**, *65*, 033311.
36. Peng, Z. A.; Peng, X. Nearly Monodisperse and Shape-Controlled CdSe Nanocrystals *via* Alternative Routes: Nucleation and Growth. *J. Am. Chem. Soc.* **2002**, *124*, 3343–3353.
37. Dai, Q.; Li, D.; Chang, J.; Song, Y.; Kan, S.; Chen, H.; Zou, B.; Xu, W.; Xu, S.; Liu, B.; *et al.* Facile Synthesis of Magic-Sized CdSe and CdTe Nanocrystals with Tunable Existence Periods. *Nanotechnology* **2007**, *18*, 405603.
38. Yu, W. W.; Wang, Y. A.; Peng, X. Experimental Determination of the Extinction Coefficient of CdTe, CdSe, and CdS Nanocrystals. *Chem. Mater.* **2003**, *15*, 2854–2860.
39. Bandaranayake, R. J.; Wen, G. W.; Lin, J. Y.; Jiang, H. X.; Sorensen, C. M. Structural Phase Behavior in II−VI Semiconductor Nanoparticles. *Appl. Phys. Lett.* **1995**, *67*, 831–833.
40. Jose, R.; Zhanpeisov, N. U.; Fukumura, H.; Baba, Y.; Ishikawa, M. Structure−Property Correlation of CdSe Clusters Using Experimental Results and First-Principles DFT Calculations. *J. Am. Chem. Soc.* **2006**, *128*, 629–636.
41. Deglmann, P.; Ahlrichs, R.; Tsereteli, K. Theoretical Studies of Ligand-Free Cadmium Selenide and Related Semiconductor Clusters. *J. Chem. Phys.* **2002**, *116*, 1585–1597.
42. Scherrer, P.; Göettingen, N. G. W. *Math. Phys. Klasse* **1918**, 98.
43. JCPDS (Joint Committee on Powder Diffraction Standards) file 06-0314.
44. Nien, Y.-T.; Zaman, Md. B.; Ouyang, J.; Chen, I.-G.; Hwang, C.-S.; Yu, K. Raman Scattering for the Size of CdSe and CdS Nanocrystals and Comparison with Other Techniques. *Mater. Lett.* **2008**, *62*, 4522–4524.